frontiers | Frontiers in Earth Science

TYPE Original Research
PUBLISHED 23 February 2024
DOI 10.3389/feart.2024.1342561

OPEN ACCESS

EDITED BY
Wenlong Ding,
China University of Geosciences, China

REVIEWED BY
Hu Li,
Southwest Petroleum University, China
Xixin Wang,
Yangtze University, China

*CORRESPONDENCE
Ruifei Wang,
sirwrf2003@163.com

RECEIVED 22 November 2023
ACCEPTED 29 January 2024
PUBLISHED 23 February 2024

CITATION
Wang R and Tang Y (2024), Study on the rock physical mechanical properties evaluation of tight oil reservoir in Chang 7 member, Longdong area, Ordos Basin, China.
Front. Earth Sci. 12:1342561.
doi: 10.3389/feart.2024.1342561

Study on the rock physical mechanical properties evaluation of tight oil reservoir in Chang 7 member, Longdong area, Ordos Basin, China

Ruifei Wang* and Ying Tang

College of Petroleum Engineering, Xi'an Shiyou University, Xi'an, China

The study aims to investigate the rock mechanical properties of the Chang 7 member tight oil reservoir in the Longdong region of the Ordos Basin, China, with the goal of enhancing the efficiency of oilfield development. Despite numerous contributions in the field of rock mechanics, challenges persist in reconciling experimental results with actual geological conditions and achieving comprehensive understanding of rock mechanical properties in tight oil reservoirs. To address this, a variety of experimental methods were employed to systematically assess the mechanical properties of the target reservoir. Rock density was measured using volumetric methods, tensile strength was evaluated through the Brazilian test, uniaxial and triaxial compression tests were conducted to assess rock mechanics properties, and dynamic elastic modulus and Poisson's ratio were obtained via sonic velocity measurements. Furthermore, differential strain analysis and imaging log analysis were employed to determine the magnitude and direction of geostress. The results revealed that fine-grained sandstone exhibited higher rock density and relatively higher tensile strength, while muddy siltstone exhibited comparatively lower values in these aspects. Analysis of the influence of confining pressure on rock mechanics properties demonstrated a strong positive correlation between compressive strength and Young's modulus with confining pressure, while Poisson's ratio exhibited more irregular variations. Additionally, a mathematical relationship between dynamic and static rock mechanical parameters was established. Lastly, based on the characteristics of geostress, reliable foundations for optimizing hydraulic fracturing and wellbore layout were provided. This study has enriched and complemented the investigation of rock mechanical properties in tight reservoirs, offering vital parameters and theoretical support for the development of tight oil reservoirs. This bears significant importance in enhancing petroleum extraction efficiency and optimizing engineering design.

KEYWORDS

Ordos Basin, Chang 7 member, tight oil reservoir, rock physical mechanical properties, experiments

1 Introduction

In the field of reservoir rock physical mechanics, previous research has covered various aspects. Key studies in this field include Gao et al. (2016), who explored rock deformation in the Lucaogou Formation in the Jimsar Sag, China, to reveal rock deformation characteristics and strength, providing a basis for establishing reservoir rock mechanics parameter logging evaluation models. Additionally, Li et al. (2022) performed triaxial stress tests on the continental mixed fine-grained sedimentary rocks in the western part of the Qaidam Basin, China, to investigate the correlation between rock mechanics properties and brittleness. Xiong et al. (2023) analyzed the rock mechanics properties of the fluvial shale reservoir of the Fengcheng Formation in the Mahu Sag, Junggar Basin, China, using reservoir logging and post-fracturing oil test data, and studied the influence of rock mechanics properties on the fracturing effect of the fluvial shale reservoir. However, despite the valuable contributions of these studies in the field of rock mechanics, there are still some limitations. Firstly, although experimental research provides valuable information about the mechanical properties and strength of rocks, there are differences between experimental conditions and actual geological conditions. Therefore, the applicability of research results in practical applications needs further validation. Secondly, the current research understanding of the rock mechanics properties of specific regions or oil and gas fields is still not comprehensive enough to serve as a basis for engineering applications. The rock physical mechanical properties play a crucial role in the development of tight oil reservoirs, which refer to oil-bearing formations with low porosity and poor permeability. Accurate assessment and understanding of rock physical mechanical parameters are essential for the efficient development of such reservoirs (Liu et al., 2009; Zhang P. et al., 2022). A comprehensive understanding of the physical-mechanical properties of rocks in tight oil reservoirs, such as elastic modulus, Poisson's ratio, compressive strength, etc., can help predict reservoir deformation behavior, fracture propagation characteristics, and oil and gas migration paths, thereby guiding the optimization of development strategies and increasing production capacity.

2 Geological backgrouond

The Chang 7 Member reservoir in the Longdong area is one of the significant targets in the Ordos Basin, China, with important potential for tight oil resources. As a large polyphase cratonic basin, the Ordos Basin has undergone overall subsidence and basin migration processes (Zhong et al., 2013; He and Yun, 2021). During its sedimentary evolution, the Chang 7 period represents the largest expansion phase of the lake basin, characterized by deep

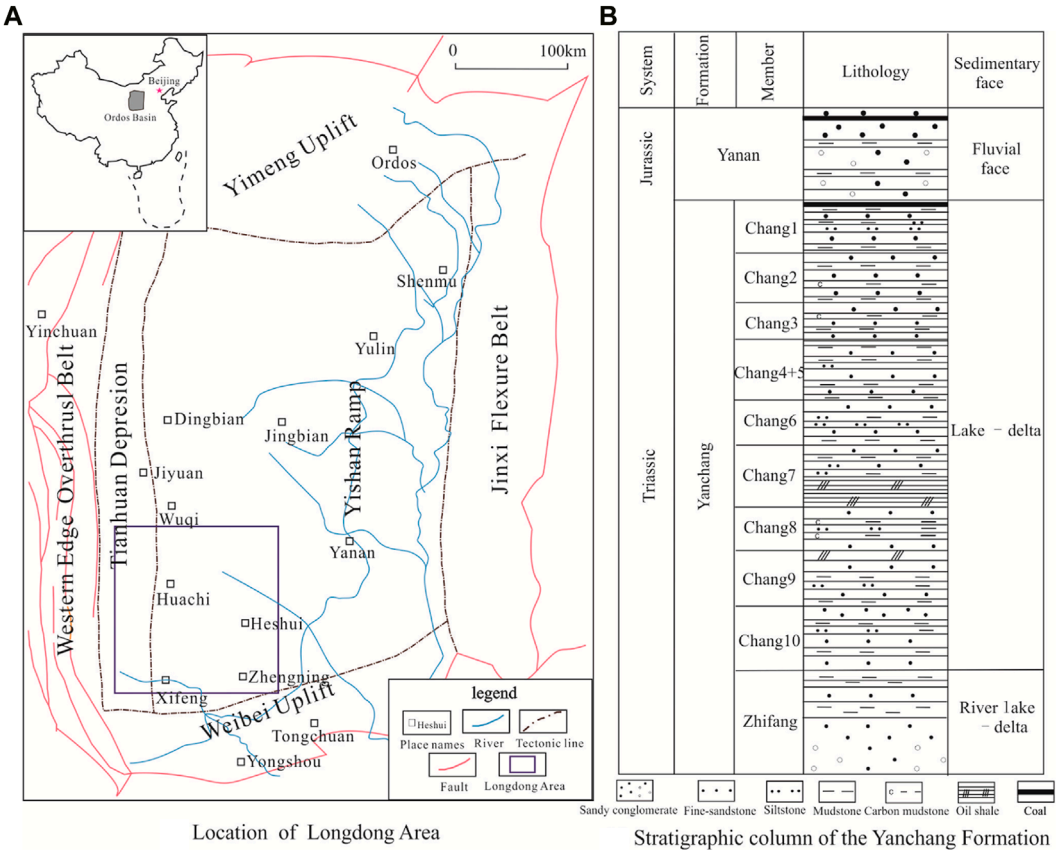

FIGURE 1
Location and stratigraphic column of the Longdong area.

and extensive water bodies, and the deposition of a nearly 100-m-thick series of oil-bearing rocks dominated by oil shale, providing the foundation for Mesozoic continental oil generation (Yang et al., 2022). The study area in the Longdong area extends from Wuqi in the north to Zhengning in the south, Zhenyuan in the west, and Ta'erwan in the east, covering an area of approximately 3×10^4 km^2 (Figure 1), with proven oil reserves reaching 5×10^8 km^2. However, due to the complex geological and rock physical mechanical properties, the development of the tight oil reservoir in the Chang 7 Member faces challenges. The rock physical mechanical properties are crucial factors in assessing reservoir's development feasibility, determining development strategies, and optimizing production efficiency. Nevertheless, the insufficient understanding of the rock physical mechanical properties of the tight oil reservoirs in the study area has constrained the targeted and effective implementation of engineering measures.

FIGURE 2
RTR-1000 high-temperature high-pressure dynamic rock triaxial testing system.

FIGURE 3
Ultrasonic rock parameter tester.

3 Methods

In this study, we conducted rock density measurements, triaxial rock mechanics experiments, acoustic experiments, and geostress tests, and collected FMI (Formation Micro-Imager) logging data.

The dry density of 33 rock samples was measured using the volumetric method. Cylindrical specimens with dimensions of Φ25×50 mm were prepared, ensuring a height-to-diameter ratio of 2.0–2.5. The dimensions of the specimens were measured, and their volumes were calculated. The specimens were then dried continuously for 1–2 days at a temperature of 105°C–110°C and cooled to room temperature. The dry mass of the specimens was measured with an accuracy of 0.01 g. The dry density was calculated using the mass and volume of the specimens.

The research employed the Brazilian tensile test to measure the tensile strength of the rocks. Firstly, the dimensions of the specimens were measured, and then the specimens were dried continuously for 1–2 days at a temperature of 105°C–110 °C and cooled to room temperature in a drying oven. Next, the specimens were accurately placed in the testing apparatus, and a relatively linear load was applied using the Brazilian tensile testing machine to induce tensile stress along the radial direction of the specimen until failure occurred, and the failure load value was recorded. Finally, the tensile strength of the rock was calculated using the formula $S_t = 2P/\pi DL$, where S_t is the tensile strength of the rock (MPa), P is the failure load (KN), D is the diameter of the specimen (cm), and L is the thickness of the specimen (cm).

The uniaxial compression test method was used to evaluate the mechanical properties of rocks. The oil and gas reservoir geostress testing system (Figure 2) was utilized as the testing instrument, and the specimens were prepared according to the standard procedures. During the test procedure, axial deformation sensors were connected, and initial values were set. The test was conducted using axial load control and radial deformation control until the specimen failed. The oil and gas reservoir geostress testing system automatically collected data on stress, strain, and other parameters. Based on relevant calculation formulas, the axial failure stress, elastic modulus, and Poisson's ratio were determined.

The rock triaxial compression test was used to study the deformation and strength characteristics of the rocks. In the high-temperature high-pressure dynamic rock triaxial testing system (Figure 2), the longitudinal and lateral deformations of the rock samples were measured under different confining pressures to obtain the elastic modulus, Poisson's ratio, and triaxial compressive strength of the rocks. The specimens were cylindrical with dimensions of Φ25×50 mm, meeting the preparation requirements. The test procedure included connecting deformation sensors, applying confining pressure, and controlling axial load and radial deformation. Computer software was used to collect and determine the elastic modulus and Poisson's ratio under different confining pressure conditions.

The ultrasonic pulse transmission method was used to conduct rock acoustic wave characterization using the ultrasonic rock parameter tester (Figure 3). By measuring the propagation time of longitudinal or transverse waves along the length direction of the specimen, the longitudinal and transverse wave velocities of the rock sample were calculated. Furthermore, using the obtained velocity values in conjunction with the sample's density, we can

TABLE 1 Rock density test results.

Well	Core number	Rock type	Depth (m)	Sample number	Diameter D (mm)	Height H (mm)	Dry weight M_d (g)	Dry density ρ_d (g/cm^3)
N25	$11\frac{9}{36}$	Fine-grained sandstone	1,407.03–1,412.42	S1-1	25.36	50.12	67.41	2.664
				S1-2	25.32	50.25	67.20	2.657
				S1-3	25.33	50.20	67.53	2.671
				S1-4	25.34	50.27	67.52	2.665
				S1-5	25.33	50.04	67.20	2.666
				S1-6	25.34	50.42	67.59	2.659
				S1-7	25.35	50.30	67.53	2.661
				S1-8	25.35	50.09	67.38	2.667
				S1-9	25.33	50.50	67.44	2.651
				S1-10	25.34	50.08	67.39	2.670
				S1-11	25.33	50	67.19	2.668
				S1-12	25.39	50.29	67.28	2.644
				Mean				**2.662**
Z43	$7\frac{57}{68}$	Fine-grained sandstone	1792.37–1801.84	S3-1	25.12	44.23	52.78	2.409
				S3-2	25.37	47.83	57.39	2.375
				S3-3	25.30	50.07	60.08	2.388
				S3-4	25.34	50.05	60.45	2.396
				S3-5	25.35	50.52	60.36	2.368
	$7\frac{33}{68}$			S3-6	25.35	50.23	62.45	2.465
				S3-7	25.34	50.02	62.30	2.471
				S3-8	25.31	49.94	61.69	2.456
				S3-9	25.30	50.02	62.41	2.483
				Mean				**2.424**
Z10	$2\frac{194}{235}$	Muddy siltstone	1758.13–1758.96	S4-1	25.36	50.07	65.89	2.607
				S4-2	25.35	50.07	65.50	2.593
				S4-3	25.34	50.05	65.19	2.584
				S4-4	25.35	50.07	66.27	2.624
				S4-5	25.34	49.96	65.15	2.587
				S4-6	25.33	49.98	65.36	2.596
				S4-7	25.31	51.33	66.82	2.589
				S4-8	25.33	50.02	65.67	2.607

(Continued on the following page)

TABLE 1 (*Continued*) Rock density test results.

Well	Core number	Rock type	Depth (m)	Sample number	Diameter D (mm)	Height H (mm)	Dry weight M_d (g)	Dry density ρ_d (g/cm^3)
				S4-9	25.33	50.01	65.63	2.606
				S4-10	25.33	50.16	65.63	2.598
				S4-11	25.36	50.53	66.14	2.593
				S4-12	25.37	50.15	65.30	2.577
				Mean				**2.597**

TABLE 2 Rock tensile strength test results.

Well	Core number	Rock type	Depth (m)	Sample number	Diameter D (mm)	Length (mm)	Maximum failure load (KN)	Tensile strength (MPa)
N25	$11\frac{9}{36}$	Fine-grained sandstone	1,407.03–1,412.42	S1P-1	2.543	2.537	7.96	7.589
				S1P-2	2.543	2.555	8.318	8.154
				S1P-3	2.532	2.538	7.706	7.638
				S1P-4	2.539	2.569	10.258	10.017
				Mean				**8.417**
Z43	$7\frac{33}{68}$	Fine-grained sandstone	1792.37–1801.84	S3P-1	2.537	2.486	3.346	3.379
				S3P-2	2.535	2.531	4.474	4.441
				S3P-3	2.536	2.560	6.528	6.045
				S3P-4	2.536	2.537	4.240	4.198
				Mean				**4.606**
Z10	$2\frac{194}{235}$	Muddy siltstone	1758.13–1758.96	S4P-1	2.538	2.612	4.738	4.552
				S4P-2	2.536	2.577	4.706	4.587
				S4P-3	2.538	2.552	2.220	2.183
				S4P-4	2.536	2.527	5.036	5.005
				Mean				**4.082**

determine the elastic modulus and Poisson's ratio of the sample under a given pressure.

The differential strain analysis test method was used to determine the direction and magnitude of geostress (Zhang X. J. et al., 2022). This method is based on the assumption that the rock mechanical properties are isotropic and utilizes the ratio relationship of principal strains to determine the magnitude of geostress. Firstly, rock samples were extracted from underground to eliminate the effect of geostresses, causing the opening of microcracks within the rocks. The direction and density of these microcracks are proportional to the pre-existing geostress state. Then, the extracted rock samples were processed into cubic rock blocks, and three strain gauges were attached to three mutually perpendicular planes at 45° angles. Subsequently, the rock samples were placed inside a pressure chamber, and three equal confining pressures were applied in different directions. Simultaneously, the strains in each direction were measured. By analyzing the principal strain features and their corresponding stress values, determine the direction and magnitude of geostresses.

TABLE 3 Rock uniaxial compression test results.

Well	Rock type	Depth (m)	Sample number	Dry density ρ_d (g/cm^3)	Uniaxial tensile strength σ_1 (MPa)	Elastic modulus E ($\times 10^4$MPa)	Poisson's ratio ν
N25	Fine-grained sandstone	1,407.28–1,412.65	S1-1	2.664	210.991	3.668	0.195
			S1-2	2.657	173.006	3.418	0.181
			S1-3	2.671	170.846	3.336	0.232
			Mean		**184.948**	**3.474**	**0.203**
Z43	Fine-grained sandstone	1792.37–1801.84	S3-1	2.409	94.81	2.013	0.286
			S3-2	2.375	84.816	1.529	0.289
			Mean		**89.813**	**1.771**	**0.288**
Z10	Muddy siltstone	1758.11–1758.92	S4-1	2.607	102.678	2.379	0.201
			S4-2	2.593	122.598	2.392	0.212
			S4-3	2.584	101.631	2.219	0.181
			Mean		**108.969**	**2.330**	**0.198**

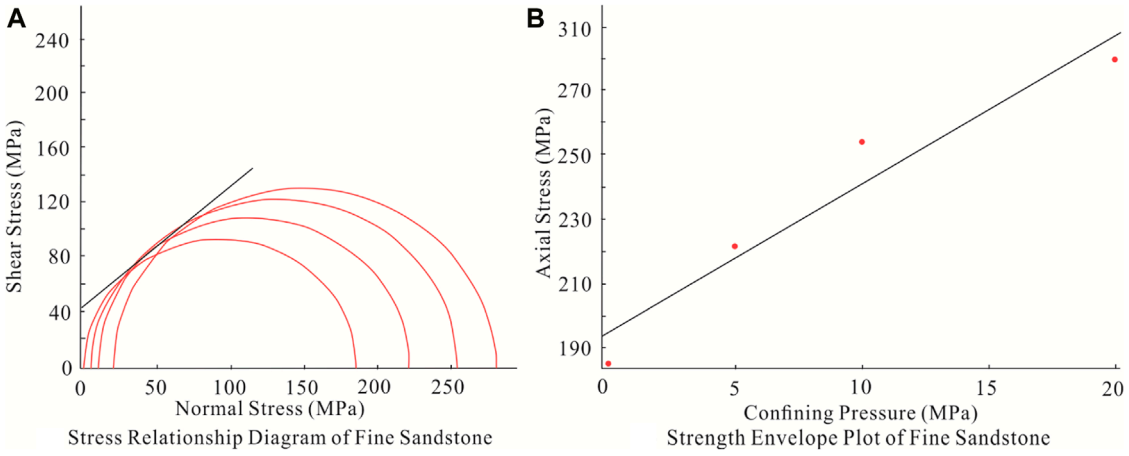

FIGURE 4
Relevant diagrams for triaxial compression (N25 well, 1,407.12m–1,412.05 m). **(A)** Stress relationship diagram of fine sandstone. **(B)** Strength envelope plot of fine sandstone.

4 Results

4.1 Rock density test

Rock density measurements were conducted using the volumetric method, which involves measuring the mass of the rock sample per unit volume after it is dried. The test results (Table 1) indicate that the average rock density of fine-grained sandstone is 2.543 g/cm^3, and the average rock density of muddy siltstone is 2.597 g/cm^3. The fine-grained sandstone in the Longdong area exhibits relatively high rock density (typically around 2.3 g/cm^3 for clastic rocks), indicating that the rocks are dense (Wang et al., 2009).

4.2 Rock tensile strength test

The maximum capacity to resist tensile failure is referred to as the rock tensile strength (Zhang et al., 2021). There are various methods for testing tensile strength, and in this experiment, the split tensile test method was used to determine the rock tensile strength. The test results (Table 2) indicate that the average tensile strength

TABLE 4 Rock triaxial compression test results.

Well	Rock type	Depth (m)	Sample number	Dry density ρ_d(g/cm^3)	Confining pressure (MPa)	Compressiv strength σ_1 (MPa)	Elastic modulus E (× 10^{4}MPa)	Poisson's ratio ν
N25	Fine-grained sandstone	1,407.28–1,412.65	S1-4	2.665	5	198.74	3.697	0.188
			S1-6	2.659		238.79	3.818	0.200
			S1-7	2.661		226.21	3.826	0.210
			Mean			**221.247**	**3.780**	**0.199**
			S1-5	2.666	10	253.86	3.886	0.226
			S1-8	2.667		263.27	3.932	0.229
			S1-9	2.651		243.95	3.899	0.223
			Mean			**253.693**	**3.906**	**0.226**
			S1-10	2.670	20	274.7	4.167	0.232
			S1-11	2.668		289.69	3.999	0.201
			S1-12	2.644		274.14	4.195	0.223
			Mean			**279.510**	**4.120**	**0.219**
Shear strength index			$\sigma_1 = \sigma_0 + k\,\sigma_3$			$\tau = c + \sigma_1 tg\,\varphi$		
Sample number N =12			σ_0 =194.304 (MPa)			k =4.633		
Correlation coefficient r =0.966			Cohesive force C =43.363 (MPa)			Internal friction angle φ =41.34 (°)		

TABLE 5 Rock triaxial compression test results.

Well	Rock type	Depth (m)	Sample number	Dry density ρ_d(g/cm^3)	Confining pressure (MPa)	Compressive strength σ_1 (MPa)	Elastic modulus E (× 10^{4}MPa)	Poisson's ratio ν
Z 43	Fine-grained sandstone	1792.37–1801.84	S3-6	2.465	5	145.16	2.336	0.270
			S3-7	2.471		145.52	2.323	0.213
			Mean			**145.340**	**2.330**	**0.242**
			S3-8	2.456	15	183.15	2.475	0.213
			S3-9	2.483		191.02	2.490	0.231
			Mean			**187.085**	**2.483**	**0.222**
			S3-3	2.388	25	197.73	2.525	0.177
			S3-4	2.396		204.58	2.556	0.175
			S3-5	2.368		202.73	2.542	0.218
			Mean			**201.680**	**2.541**	**0.190**
Shear strength index			$\sigma_1 = \sigma_0 + k\,\sigma_3$			$\tau = c + \sigma_1 tg\,\varphi$		
Sample number N =9			σ_0 =108.511 (MPa)			k =4.219		
Correlation coefficient r =0.932			Cohesive force C =23.626 (MPa)			Internal friction angle φ =40.59 (°)		

TABLE 6 Rock triaxial compression test results.

Well	Rock type	Depth (m)	Sample number	Dry density ρ_d(g/cm^3)	Confining pressure (MPa)	Compressive strength σ_1 (MPa)	Elastic modulus E ($\times 10^4$MPa)	Poisson's ratio ν
Z10	Muddy siltstone	1758.11–1758.92	S4-7	2.589	5	102.77	2.303	0.181
			S4-8	2.607		146.16	2.451	0.189
			S4-9	2.606		97.86	2.213	0.195
			Mean			**115.597**	**2.322**	**0.188**
			S4-10	2.598	15	134.7	2.385	0.182
			S4-11	2.593		189.13	2.384	0.239
			S4-12	2.577		188.71	2.493	0.196
			Mean			**170.847**	**2.421**	**0.206**
			S4-4	2.624	25	202.53	2.519	0.188
			S4-5	2.587		211.76	2.457	0.213
			S4-6	2.596		204.80	2.553	0.237
			Mean			**206.363**	**2.510**	**0.213**
Shear strength index			$\sigma_1 = \sigma_0 + k\,\sigma_3$			$\tau = c + \sigma_1 \mathrm{tg}\,\varphi$		
Sample number N =12			σ_0 =103.772 (MPa)			k =4.418		
Correlation coefficient r =0.989			Cohesive force C =25.075 (MPa)			Internal friction angle φ =38.06 (°)		

of fine-grained sandstone is 6.43 MPa, while the average tensile strength of muddy siltstone is 4.08 MPa.

4.3 Rock uniaxial compression test

Rock uniaxial compression testing involves measuring the longitudinal and lateral deformations of regular-shaped rock specimens under uniaxial pressure to determine the rock's elastic modulus, Poisson's ratio, and uniaxial compressive strength (Gao et al., 2022; Zhao et al., 2023). The test results (Table 3) indicate that the average compressive strength of fine-grained sandstone is 137.38 MPa, the average elastic modulus is 2.623×10^4 MPa, and the average Poisson's ratio is 0.246. For muddy siltstone, the average compressive strength is 108.969 MPa, the average elastic modulus is 2.330×10^4 MPa, and the average Poisson's ratio is 0.198.

4.4 Rock triaxial compression test

The purpose of rock triaxial compression test is to understand the deformation and strength characteristics of rocks under complex stress conditions. The experiment provides mechanical parameters and the Mohr circle envelope (Figure 4) for rocks under different pressure conditions. The Mohr circle envelope represents the enveloping circle of the maximum principal stress and can fully describe the failure characteristics of rocks under any stress state, enabling the determination of the internal friction angle and cohesion of the rocks (Chen et al., 2021; Wang et al., 2023). By measuring the longitudinal and lateral deformations of regularly-shaped rock specimens under different confining pressures, the elastic modulus, Poisson's ratio, and triaxial compressive strength of the rocks were determined. In this experiment, the equal lateral pressure triaxial compression test ($\sigma_1>\sigma_2=\sigma_3$) was conducted to simulate real geological conditions (Wang S. L. et al., 2022; Li, 2022). The loading pressure levels were determined based on the lithology and depth. The test results (Table 4–6) indicate that the average cohesion of fine-grained sandstone is 28.6 MPa, and the internal friction angle is 45.7°. For muddy siltstone, the average cohesion is 25.075 MPa, and the internal friction angle is 38.06°.

4.5 Rock acoustic properties test

Using ultrasonic pulse transmission method, the propagation time of longitudinal or transverse waves along the sample length direction is measured (Figure 5), and the longitudinal and transverse wave velocities of the sample are calculated to obtain the elastic modulus and Poisson's ratio of the sample under a given confining pressure. (Liu et al., 2009; Zuo et al., 2011; Han et al., 2017). The rock acoustic properties test (Table 7) demonstrates that with the increase of confining pressure, both longitudinal and transverse wave velocities, as well as the elastic modulus, increase.

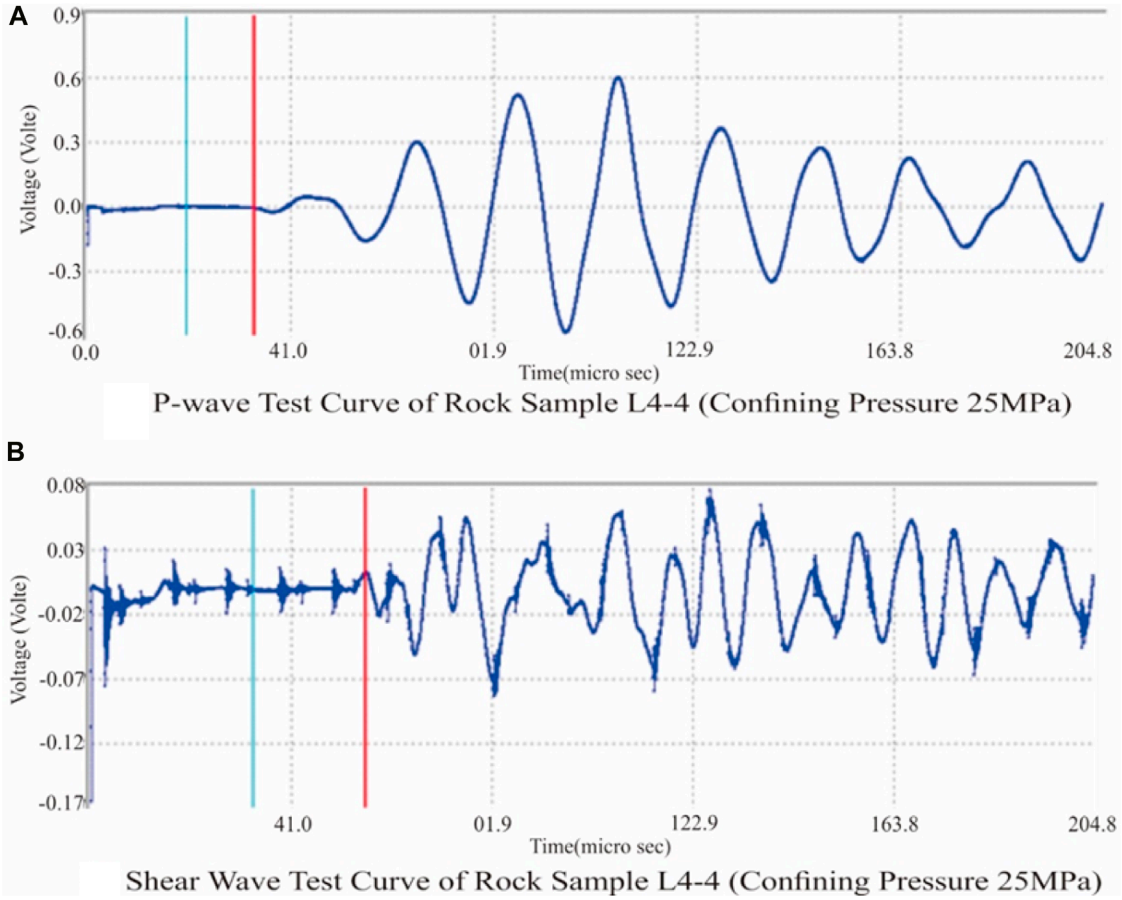

FIGURE 5
P-wave and shear wave test curve of rock sample L4-4. **(A)** P-wave **(B)** Shear wave.

4.6 Magnitude of geostress and its well logging evaluation

In this study, a total of 8 core samples underwent differential strain testing and analysis. The test results (Table 8) indicate that the vertical principal stress gradient is 0.025 MPa/m, the average gradient of the maximum horizontal principal stress gradient is 0.020 MPa/m, and the average gradient of the minimum horizontal principal stress gradient is 0.016 MPa/m. The results of the differential strain test show that the vertical principal stress is greater than the maximum horizontal principal stress.

5 Discussion

5.1 The influence of confining pressure on mechanical parameters in rocks

5.1.1 The influence of confining pressure on compressive strength in rocks

Analyzing the influence of confining pressure on compressive strength, it is observed that there is a positive correlation between the compressive strength of the rock and the confining pressure (Figure 6A). According to the Mohr-Coulomb criterion, during the compressive failure of the rock under confining pressure (σ_3), it satisfies the following relationship with the maximum axial stress (σ_1):

$$\sigma_1 = K^2\sigma_3 + 2CK$$

In the equation, K = ctg (45°-θ/2);
θ—the internal friction angle of the rock, °;
C—the cohesion of the rock, MPa.

When the rock reaches critical failure, σ_1 represents the triaxial compressive strength of the rock. Since the internal friction angle and cohesion are inherent properties of the rock and independent of confining pressure, the compressive strength of the rock under triaxial compression will increase linearly with the increase in confining pressure (Duan et al., 2023).

5.1.2 The influence of confining pressure on Young's modulus in rocks

Analyzing the influence of confining pressure on Young's Modulus, it can be observed that the Young's modulus increases with the increase in confining pressure (Figure 6B). Due to the confinement's limiting effect on strain, as the confining pressure increases, the axial strain decreases under the same axial stress

TABLE 7 Rock acoustic properties test results.

Well	Rock type	Depth (m)	Sample number	Dry density ρ_d(g/cm^3)	Confining pressure (MPa)	P-wave velocity (m/s)	Shear wave velocity (m/s)	Elastic modulus E (× 10^4MPa)	Poisson's ratio ν
N25	Fine-grained sandstone	1,407.28–1,412.65	S1-4	2.665	5	4,511	2,749	4.848	0.20
			S1-6	2.659		4,175	2,464	3.979	0.23
			S1-7	2.661		4,374	2,486	4.146	0.26
			Mean			**4,353**	**2,566**	**4.324**	**0.230**
			S1-5	2.666	10	4,581	2,804	5.030	0.20
			S1-8	2.667		4,356	2,512	4.201	0.25
			S1-9	2.651		4,247	2,533	4.162	0.22
			Mean			**4,394**	**2,616**	**4.464**	**0.223**
			S1-10	2.670	20	4,585	2,595	4.543	0.26
			S1-11	2.668		4,460	2,591	4.457	0.25
			S1-12	2.644		4,486	2,687	4.654	0.22
			Mean			**4,510**	**2,624**	**4.551**	**0.243**
Z43	Fine-grained sandstone	1792.37–1801.84	S3-6	2.465	5	3,492	1961	2.404	0.27
			S3-7	2.471		2,916	1883	2.000	0.14
			Mean			**3,204**	**1922**	**2.202**	**0.205**
			S3-8	2.456	15	3,654	2,177	2.852	0.22
			S3-9	2.483		3,623	2,182	2.871	0.22
			Mean			**3,639**	**2,180**	**2.862**	**0.220**
			S3-3	2.388	25	3,831	2,273	3.029	0.23
			S3-4	2.396		4,048	2,481	3.535	0.20
			S3-5	2.368		3,781	2,293	3.009	0.21
			Mean			**3,887**	**2,349**	**3.191**	**0.213**
Z10	Muddy siltstone	1758.11–1758.92	S4-7	2.589	5	3,498	2093	2.767	0.22
			S4-8	2.607		3,477	2089	2.768	0.22
			S4-9	2.606		3,408	2048	2.659	0.22
			Mean			**3,461**	**2077**	**2.731**	**0.220**
			S4-10	2.598	15	3,559	2,105	2.832	0.23
			S4-11	2.593		3,585	2,148	2.916	0.22
			S4-12	2.577		3,672	2,105	2.865	0.26
			Mean			**3,605**	**2,119**	**2.871**	**0.237**

(Continued on the following page)

TABLE 7 (*Continued*) Rock acoustic properties test results.

Well	Rock type	Depth m)	Sample number	Dry density ρ_{d}(g/cm^{3})	Confining pressure (MPa)	P-wave velocity (m/s)	Shear wave velocity (m/s)	Elastic modulus E (× 10^{4}MPa)	Poisson's ratio ν
			S4-4	2.624	25	3,666	2,184	3.063	0.22
			S4-5	2.587		4,238	2,310	3.557	0.29
			S4-6	2.596		3,862	2,222	3.209	0.25
			Mean			**3,922**	**2,239**	**3.279**	**0.253**

TABLE 8 Ground stress values.

Well	Depth (m)	Stress gradient (MPa/m)			Principal stress value (MPa)		
		Vertical	Horizontal maximum	Horizontal minimum	Vertical	Horizontal maximum	Horizontal minimum
Y206	1962.64–1969.41	0.0230	0.0193	0.0173	45.22	37.94	34.01
Y34	1972.37–1976.48	0.0240	0.0196	0.0166	47.42	38.73	32.80
Y 37	2,354.36–2,360.90	0.0250	0.0190	0.0170	58.93	44.78	40.07
Z133	1977.82–1994.02	0.0249	0.0195	0.0156	49.43	38.71	30.97
N25	1,452.14–1,455.81	0.0251	0.0198	0.0154	36.45	28.75	22.36
B107	1722.32–1791.05	0.0252	0.0203	0.0159	45.13	36.36	28.48
Z176	1,516.46–1,533.94	0.0250	0.0203	0.0155	38.13	30.96	25.16
Z233	1735.50–1738.04	0.0249	0.0197	0.0160	43.20	34.18	27.76
Mean		0.025	0.020	0.016	45.49	36.30	30.20

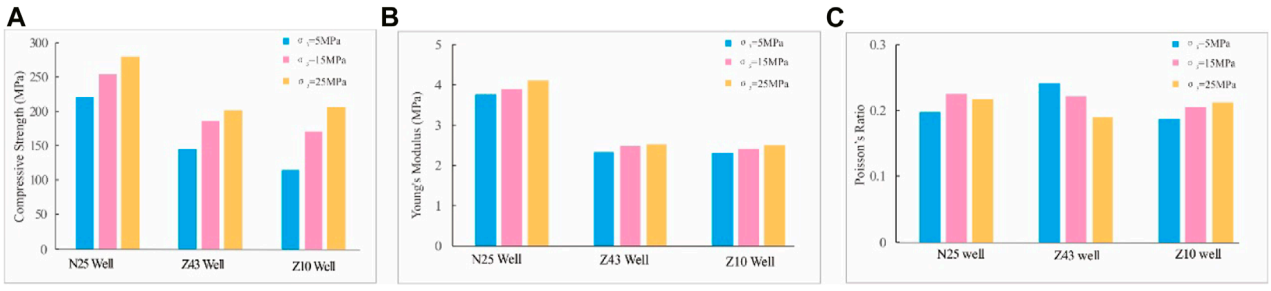

FIGURE 6
The influence of confining pressure on rock mechanics parameters. **(A)** Confining pressure—compressive strength; **(B)** Confining pressure—Young's modulus; **(C)** Confining pressure—Poisson's ratio.

(Wang et al., 2016) (Figure 7). Consequently, Young's modulus increases with the increase in confining pressure.

5.1.3 The influence of confining pressure on Poisson's ratio in rocks

Analyzing the influence of confining pressure on Poisson's Ratio, it can be observed that with the increase in confining pressure, the Poisson's ratio of the N25 well sample first increases and then decreases (Figure 6C). For the Z43 well sample, the Poisson's ratio decreases with the increase in confining pressure, while for the Z10 well sample, the Poisson's ratio increases with the increase in confining pressure. From the figures, it is evident that under the same axial stress, with the increase in confining pressure, both axial strain and radial strain decrease, but the reduction ratio is not

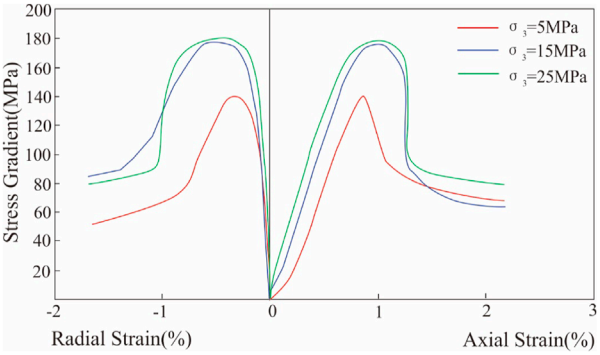

FIGURE 7
Triaxial compression stress-strain curves of Z43 well samples at different confining pressures.

consistent. This irregular variation in Poisson's ratio is attributed to the effects of pore and microcrack closure.

5.2 Correlation between dynamic and static rock mechanical parameters

The rock triaxial compression test can provide static elastic parameters, while the rock acoustic wave test can provide dynamic elastic parameters. By utilizing the correlation between dynamic and static elastic parameters, dynamic elastic parameters obtained from logging and other methods can be converted into static elastic parameters (Zhong, et al., 2012; Wang, et al., 2020). This approach not only avoids expensive experimental costs but also allows obtaining continuous static elastic parameter values. Analyzing the relationship between dynamic elastic modulus and static elastic modulus, the mathematical relationship can be derived (Figure 8):

The static elastic modulus is 0.9015, the dynamic elastic modulus is 0.0489, and the correlation coefficient between them is 84.41%.

It can be inferred that the dynamic and static Young's moduli have a strong correlation. Furthermore, by analyzing the acoustic data from wells N25, Z43, and Z10, it is evident that with the increase in confining pressure, both longitudinal and transverse wave velocities, as well as elastic modulus, increase. Additionally, the mutual comparison of dynamic and static mechanical parameters of rocks can enhance the effectiveness of their utilization in oilfield development.

5.3 Impact of present-day geostress orientation on development

In oilfield development, the present-day geostress plays a crucial role as it represents the internal stress state within the crust. It is composed of factors such as formation gravity, formation pressure, tectonics, and pore fluids. Accurate understanding of stress orientation is of paramount importance for devising hydraulic fracturing and optimizing injection-production well layouts in development projects (Ge, et al., 1998; Zu, et al., 2014; Wang, et al., 2022b).

In this study, the orientation of drilling-induced fractures was directly determined using Formation Micro-Imaging (FMI) technology to ascertain the maximum principal geostress direction (Figure 9). This technique utilizes drilling-induced fractures formed during the drilling process to determine the direction of geostress. Due to the anisotropy of horizontal stress in geological formations, it results in the formation of maximum and minimum stress vector fields in the horizontal direction. The direction of the drilling-induced fractures corresponds to the direction of maximum horizontal geostress in the formation. Analysis of well Z233 in the study area revealed that the direction of maximum horizontal principal stress ranged from 77° to 98°, with an average of 95°, aligning closely with an east-west direction (Figure 9).

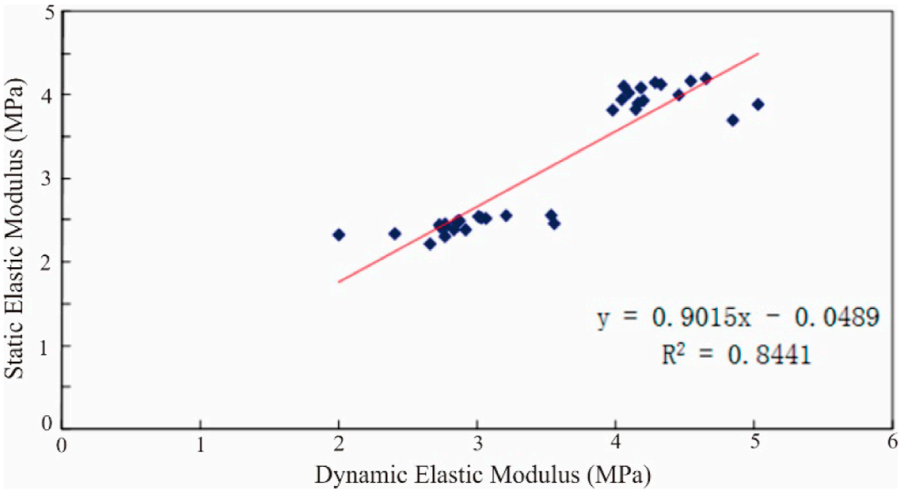

FIGURE 8
Relationship between static elastic modulus and dynamic elastic modulus.

Well	Imaging log photos of drilling-induced fractures	Maximum Principal Stress (NE)	Minimum Principal Stress (NE)	Fracture Rose Diagram
Z233	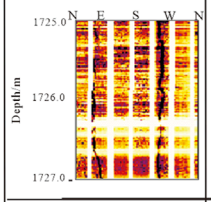	85.82°	175.82°	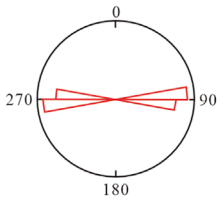
	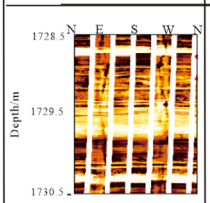	77.45°	167.45°	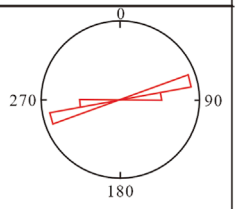
	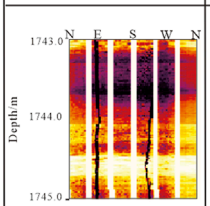	98.04°	188.04°	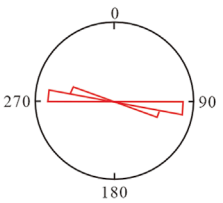
	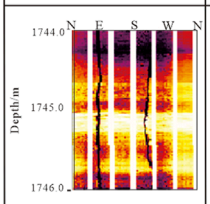	98.01°	188.01°	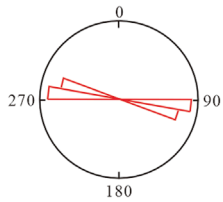
	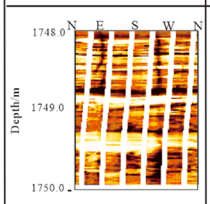	81.63°	171.63°	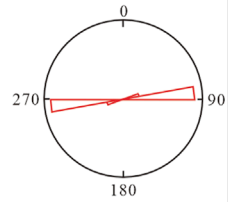
	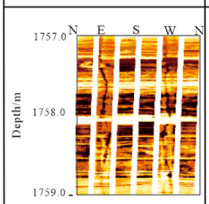	91.06°	181.06°	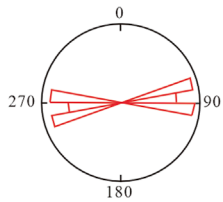
	Mean	96.25°	186.25°	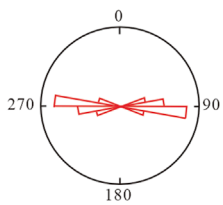

FIGURE 9
Geostress direction determined from drilling-induced fractures in well Z233.

The Chang 7 member reservoir in the study area is a tight sandstone reservoir with poor properties and limited natural fractures, making hydraulic fracturing a critical production enhancement technique. In hydraulic fracturing, the morphology and extension of induced fractures are influenced by the geostress. Generally, these fractures are perpendicular to the minimum

horizontal principal geostress and aligned with the maximum horizontal principal geostress. Consequently, fractures resulting from hydraulic fracturing also exhibit an east-west distribution. Due to the alignment of hydraulic fractures with the direction of maximum principal geostress, fluid flow within fractures will be dominant along this direction. Hence, post-fracturing well layout should consider the direction of maximum fluid flow. For tight sandstone reservoirs, the direction of hydraulic fractures corresponds to the direction of maximum fluid flow. Therefore, in well network design, the direction of maximum principal stress should be the primary consideration to achieve effective oil and gas production.

Conclusion

1) Experimental analysis of the Chang 7 tight oil reservoir in Longdong shows rock densities of 2.543 g/cm^3 for fine sandstone and 2.597 g/cm^3 for muddy siltstone, with tensile strengths of 6.43 MPa and 4.08 MPa, respectively. Uniaxial compression tests reveal compressive strengths of 137.38 MPa for fine sandstone and 108.969 MPa for muddy siltstone, while triaxial tests highlight key mechanical parameters such as elastic modulus and Poisson's ratio.
2) The study finds a strong positive correlation between compressive strength, Young's modulus, and confining pressure. However, Poisson's ratio varies irregularly with confining pressure. This relationship between dynamic and static mechanical parameters suggests a method for estimating static elastic parameters from well log data.
3) Employing differential strain and imaging well log techniques, the study determines the magnitude and orientation of geostress. This information is crucial for optimizing oilfield fracturing processes and planning well network layouts.

Data availability statement

The original contributions presented in the study are included in the article/Supplementary Material, further inquiries can be directed to the corresponding author.

Author contributions

RW: Investigation, Resources, Writing–review and editing. YT: Writing–original draft.

Funding

The author(s) declare that no financial support was received for the research, authorship, and/or publication of this article.

Conflict of interest

The authors declare that the research was conducted in the absence of any commercial or financial relationships that could be construed as a potential conflict of interest.

Publisher's note

References

Chen, G. Q., Li, H., Wei, T., and Zhu, J. (2021). Searching for multistage sliding surfaces based on the discontinuous dynamic strength reduction method. *Eng. Geol.* 286 (4), 106086. doi:10.1016/j.enggeo.2021.106086

Duan, S. Q., Sun, Y. D., Xiong, J. C., and Gao, P. (2023). A review of research on the criteria of high geostress and its influencing factors. *Chin. J. Under. Space Eng.* 19 (3), 1038–1050.

Gao, Y., Guo, P., Li, X., Li, Y. Y., Xu, D. S., Zou, Z. Y., et al. (2022). Investigation of triaxial compression failure and acoustic emission characteristics of different reservoir rocks. *J. Eng. Geol.* 30 (4), 1169–1178. doi:10.13544/j.cnki.jeg.2022-0177

Gao, Y., Wang, Y. W., Wang, Y. D., Xie, T. S., Liu, G., and Wang, L. (2016). Rock mechanics characteristics of Lucaogou tight oil reservoir in jimusaer Sag, Junggar Basin. *Xinjiang Pet. Geol.* 37 (2), 158–162. doi:10.7657/xjpg20160206

Ge, H. K., Lin, Y. S., and Wang, S. C. (1998). Geostresses determination technique and its applications in petroleum exploration and development. *J. Univ. Pet. Chin. Ed. Nat. Sci.* 22 (1), 94–99.

Han, W. G., Xiao, J., Cui, Z. D., Si, K., Wang, B. N., and Zhang, J. Y. (2017). Acoustic emission characteristics of tight sandstone during failure processes with different confining pressures. *J. Eng. Geol.* 25 (5), 1270–1278. doi:10.13544/j.cnki.jeg.2017.05.012

He, T. P., and Yun, Y. P. (2021). A comparative study on the composition of clastic and the parent rock of the source area in the yanchang Formation in the Longdong area of the Ordos Basin. *Earth Sci.* 110 (2), 64–69. doi:10.11648/j.earth.20211002.13

Li, H. (2022). Research progress on evaluation methods and factors influencing shale brittleness: a review. *Energy Rep.* 8, 4344–4358. doi:10.1016/j.egyr.2022.03.120

Li, X., Wang, K. Y., Wang, J. G., Yang, S. Y., Zhang, Q. H., and Zhang, Q. (2022). Impact of lithologic heterogeneity on brittleness of cenozoic unconventional reservoirs (Fine-Grained) in western Qaidam Basin. *Miner* 12 (11), 1443. doi:10.3390/min12111443

Liu, J. P., Wang, H. Y., Yang, Y. J., and Li, Y. H. (2009). Experimental study on different rock locating algorithms with acoustic emission. *J. Northeast. Univ. Nat. Sci.* 30 (8), 1193–1196. doi:10.1360/972009-1549

Liu, Z., Shi, B., Ge, T., Sui, F., Wang, Y., Zhang, P., et al. (2022). Tight sandstone reservoir sensitivity and damage mechanism analysis: a case study from Ordos Basin, China and implications for reservoir damage prevention. *Energy Geosci.* 3 (4), 394–416. doi:10.1016/j.engeos.2021.05.001

Wang, P. T., Liu, C., Ma, C., Ren, F. H., and Cai, M. F. (2023). On the anisotropic mohr-coulomb criterion of fractured rock masses based on the discrete fracture network. *Chin. J. Rock Mech. Eng.* 42 (S1), 3266–3280. doi:10.13722/j.cnki.jrme.2022.0627

Wang, S., Dai, J. S., Fu, X. L., Wang, Y., Chen, G. Q., and Xu, F. G. (2016). Numerical simulation research on current stress of Es3 of the 5th block of bonan oilfield and analysis of its influence factors. *Pet. Geol. Recovery Effic.* 23 (3), 26–32. doi:10.13673/j.cnki.cn37-1359

Wang, S. L., Li, H., Lin, L. F., and Yin, S. (2022a). Development characteristics and finite element simulation of fractures in tight oil sandstone reservoirs of yanchang Formation in western Ordos Basin. *Front. Earth Sci.* 9, 823855. doi:10.3389/feart.2021.823855

Wang, X. H., Feng, Z. C., and Liu, Z. H. (2009). Study on distribution laws of rock density. *Chin. J. Rock Mech. Eng.* 28 (A02), 3484–3489. doi:10.3321/j.issn:1000-6915.2009.z2.029

Wang, X. X., Hou, J. G., Li, S. H., Dou, L. X., Song, S. H., Kang, Q. Q., et al. (2020). Insight into the nanoscale pore structure of organic-rich shales in the bakken formation, USA. *J. Pet. Sci. Eng.* 191, 107182. doi:10.1016/j.petrol.2020.107182

Wang, X. X., Yu, S. Y., Li, S. H., and Zhang, N. D. (2022b). Two parameter optimization methods of multi-point geostatistics. *J. Pet. Sci. Eng.* 208, 109724. doi:10.1016/j.petrol.2021.109724

Xiong, J., Wu, J., Liu, X. J., Zhang, L., and Liang, L. X. (2023). Investigation on the geomechanical characteristics of the continental shale reservoirs and its influence on the fracturing effect. *J. Southwest Pet. Univ. Sci. Technol. Ed.*, doi:10.11885/j.issn.1674.5086.2021.12.28.01

Yang, J. R., Liu, X. Y., and Xu, W. L. (2022). Reservoir forming dynamics of differential accumulation of tight oil in the yanchang formation Chang 8 member in the Longdong area, Ordos Basin, Central China. *Front. Earth Sci.* 9, 1414. doi:10.3389/feart.2021.788826

Zhang, K. S., Tang, M. R., Wang, C. W., Wang, G. T., Dou, L. B., and Sun, H. B. (2021). Study on prediction method of tensile strength for tight sandstone formation. *Prog. Geophys.* 36 (1), 318–324. doi:10.6038/pg2021EE0076

Zhang, P., Xu, D., Fu, X., Xie, J., Dong, Y., and Zhang, X. (2022a). Evaluation of hydraulic conductivity based on fault confinement studies. *J. Min. Strata Control Eng.* 4 (2), 23–33. doi:10.13532/j.jmsce.cn10-1638/td.20211215.001

Zhang, X. J., He, J. H., Xu, Q. L., Ye, T. R., Deng, H. C., Xu, Z. Q., et al. (2022b). Distribution characteristics and disturbance mechanism of present geostress field in the second member of xujiahe Formation in hechuan area. *Min. Petrol.* 42 (4), 71–82. doi:10.19719/j.cnki.1001-6872.2022.04.07

Zhao, Z., Shou, Y. D., and Zhou, X. P. (2023). Microscopic cracking behaviors of rocks under uniaxial compression with microscopic multiphase heterogeneity by deep learning. *Int. J. Min. Sci. Technol.* 33 (4), 411–422. doi:10.1016/j.ijmst.2022.12.008

Zhong, D. K., Zhou, L. J., Sun, H. T., Yao, J. L., Liu, X. Y., Luo, A. X., et al. (2013). Petrology of sandstone reservoirs in Longdong area, Ordos Basin. *Earth Sci. Front.* 20 (2), 52–60.

Zhong, D. K., Zhou, L. J., Sun, H. T., Yao, J. L., Ma, S. Y., and Zhu, H. H. (2012). Influences of petrologic features on diagenesis and pore development: an example from the triassic yanchang Formation in Longdong area, Ordos Basin. *Oil Gas. Geol.* 33 (6), 890–899. doi:10.11743/ogg20120610

Zu, K. W., Zeng, L. B., Liu, X. Z., Zhang, J. H., Zhao, X. Y., and Liu, G. P. (2014). Analysis of influencing factors for Ground stress in channel sandstone. *J. Geomech.* 20 (2), 149–158. doi:10.3969/j.issn.1006-6616.2014.02.006

Zuo, J. P., Pei, J. L., Liu, J. F., Peng, R. D., and Li, Y. C. (2011). Investigation on acoustic emission behavior and its time-space evolution mechanism in failure process of coal-rock combined body. *Chin. J. Rock Mech. Eng.* 30 (8), 1564–1570. doi:10.1631/jzus.B1000185